Geosci. Model Dev., 11, 2049–2066, 2018
https://doi.org/10.5194/gmd-11-2049-2018

Geoscientific Model Development
Open Access
EGU

An advanced method of contributing emissions to short-lived chemical species (OH and HO_2): the TAGGING 1.1 submodel based on the Modular Earth Submodel System (MESSy 2.53)

Vanessa S. Rieger[1,a], **Mariano Mertens**[1], **and Volker Grewe**[1,a]

[1]Deutsches Zentrum für Luft- und Raumfahrt, Institut für Physik der Atmosphäre, Oberpfaffenhofen, Germany
[a]also at: Delft University of Technology, Aerospace Engineering, Section Aircraft Noise
and Climate Effects, Delft, the Netherlands

Correspondence: Vanessa S. Rieger (vanessa.rieger@dlr.de)

Received: 13 September 2017 – Discussion started: 25 October 2017
Revised: 19 April 2018 – Accepted: 30 April 2018 – Published: 5 June 2018

Abstract. To mitigate the human impact on climate change, it is essential to determine the contribution of emissions to the concentration of trace gases. In particular, the source attribution of short-lived species such as OH and HO_2 is important as they play a crucial role for atmospheric chemistry. This study presents an advanced version of a tagging method for OH and HO_2 (HO_x) which attributes HO_x concentrations to emissions. While the former version (V1.0) only considered 12 reactions in the troposphere, the new version (V1.1), presented here, takes 19 reactions in the troposphere into account. For the first time, the main chemical reactions for the HO_x chemistry in the stratosphere are also regarded (in total 27 reactions). To fully take into account the main HO_2 source by the reaction of H and O_2, the tagging of the H radical is introduced. In order to ensure the steady-state assumption, we introduce rest terms which balance the deviation of HO_x production and loss. This closes the budget between the sum of all contributions and the total concentration. The contributions to OH and HO_2 obtained by the advanced tagging method V1.1 deviate from V1.0 in certain source categories. For OH, major changes are found in the categories biomass burning, biogenic emissions and methane decomposition. For HO_2, the contributions differ strongly in the categories biogenic emissions and methane decomposition. As HO_x reacts with ozone (O_3), carbon monoxide (CO), reactive nitrogen compounds (NO_y), non-methane hydrocarbons (NMHCs) and peroxyacyl nitrates (PAN), the contributions to these species are also modified by the advanced HO_x tagging method V1.1. The contributions to NO_y, NMHC and PAN show only little change, whereas O_3 from biogenic emissions and methane decomposition increases in the tropical troposphere. Variations for CO from biogenic emissions and biomass burning are only found in the Southern Hemisphere.

1 Introduction

The radicals hydroxyl (OH) and hydroperoxyl (HO_2) are crucial for atmospheric chemistry. Both radicals are very reactive and have a lifetime of only a few seconds. OH is frequently converted to HO_2 and vice versa. Thus, OH and HO_2 radicals are closely linked and often referenced together as the chemical family HO_x. The ratio of OH to HO_2 in an air parcel strongly depends on the chemical background, in particular on the composition of nitrogen oxides NO_x ($= NO + NO_2$) and non-methane hydrocarbons (NMHC) (Heard and Pilling, 2003).

HO_x impacts global warming and local air quality in various ways: by reacting with greenhouse gases such as methane (CH_4) and ozone (O_3), OH reduces their atmospheric residence time (e.g. Stevenson et al., 2006; Voulgarakis et al., 2013; Righi et al., 2015). Hence, HO_x controls the impact of CH_4 and O_3 on global warming. Moreover, being the main oxidizer in the troposphere, OH is involved in the decomposition of pollutants and in the production of ground-level ozone, photochemical smog and secondary organic aerosols (e.g. Lawrence et al., 2001; Heard and Pilling, 2003). Consequently, to quantify the human impact on cli-

mate and air quality, it is essential to understand the distribution and variability of OH and HO_2 in the atmosphere.

However, the determination of OH and HO_2 concentrations in the atmosphere is still challenging due to their short lifetimes. In field campaigns HO_x concentrations are measured on a local scale, which is generally difficult to compare with global models (e.g. Ren et al., 2003; Olson et al., 2006). For certain environments, such as the marine boundary layer, model studies compare well with measurements. Other regions, such as unpolluted forest areas, show large discrepancies (Heard and Pilling, 2003; Stone et al., 2012). On regional and global scales, no direct HO_x measurements are available. So far, OH concentration and its inter-annual variability can only be estimated indirectly by measurements and emission rates of methyl chloroform (CH_3CCl_3) (Prinn et al., 2005; Montzka et al., 2011). As emissions of CH_3CCl_3 steadily decline, Liang et al. (2017) suggest an alternative method: they combine several trace gases such as CH_2F_2, CH_2FCF_3, CH_3CHF_2 and $CHClF_2$ in a gradient-trend-based two-box model approach to derive a global OH concentration of 11.2×10^5 molec cm^{-3}. Overall, global chemistry climate models estimate a tropospheric OH concentration of around 11×10^5 molec cm^{-3} (Naik et al., 2013), which compares well with the observation-based results from Prinn et al. (2005) and Liang et al. (2017).

To mitigate the human impact on climate change or pollution in general, it is crucial to determine the contribution of an emission sector to the concentration of certain chemical species (Grewe et al., 2012; Clappier et al., 2017). To do so, we use a "tagging" method: the theoretical framework of this tagging method is given in Grewe et al. (2010) and Grewe (2013), and the implementation is described in Grewe et al. (2017). This method splits up all chemical species which are important for O_3 production and destruction into 10 source categories: emissions from anthropogenic non-traffic (e.g. industry and households), road traffic, shipping, aviation, biogenic sources, biomass burning, lightning, methane (CH_4) and nitrous oxide (N_2O) decompositions and stratospheric ozone production. Subsequently, the contributions of these sources to the concentrations of O_3, CO, OH, HO_2, peroxyacyl nitrates (PANs), reactive nitrogen compounds (NO_y, e.g. NO, NO_2, HNO_4) and non-methane hydrocarbons (NMHC) are diagnosed. The contribution calculations are based on chemical reaction rates, online emissions (e.g. lightning), offline emissions (e.g. road traffic) and deposition rates. Emissions of NO and NO_2 contribute to the NO_y concentration, while emissions of e.g. C_2H_4, C_3H_6 and HCHO contribute to the NMHC concentration. This tagging method considers the competition of NO_y, CO and NMHC in producing and destroying O_3.

The tagging method of the long-lived species O_3, CO, PAN, NO_y and NMHC and of the short-lived species OH and HO_2 is based on the same principles of apportioning the contributions. (In this study, O_3, CO, PAN, NO_y and NMHC are denoted as long-lived species because their atmospheric lifetime is significantly longer then the lifetime of OH and HO_2.) However, the implementation for long-lived and short-lived species differs. For the long-lived species, each source tracer is transported, receives the corresponding online or offline emissions, is deposited and reacts with other species. Based on these processes, the tagging method determines the concentration of the source tracers. A detailed description of the implementation of the tagging method for long-lived species is given in Grewe et al. (2017).

However, the short-lived species HO_x are not transported and experience neither emission nor deposition. Thus, the same implementation of the tagging method as for long-lived species is not possible. Tsati (2014) and Grewe et al. (2017) introduced a modified approach for tagging HO_x: since the lifetime of OH and HO_2 is very short, a steady state between the production and destruction of OH and HO_2 is assumed. Using the main chemical reactions of HO_x chemistry, the contributions of each source category to OH and HO_2 are determined.

The contributions to long-lived and short-lived species are closely linked (see Fig. 1). For example, the reaction

$$OH + O_3 \longrightarrow HO_2 + O_2$$

involves the long-lived species O_3 and the short-lived species OH and HO_2. Hence, this reaction is considered in the implementation of the tagging method for long-lived and short-lived species. The contribution of, for example, shipping emissions to O_3 influences the contribution of shipping emissions to HO_2: the higher the contribution to O_3, the more HO_2 is attributed to shipping emissions. Furthermore, OH from shipping emissions destroys O_3 and thus reduces the contribution of shipping emissions to O_3.

The implementation of the tagging method for the short-lived species HO_x, presented by Grewe et al. (2017), is referred to as the HO_x tagging method V1.0. It did not consider all relevant reactions for the production and loss of HO_x. In particular, the reactions which are important in the stratosphere were not taken into account. Moreover, the steady-state assumption between HO_x production and loss was not fulfilled. In this study, we present a revised version V1.1 of the HO_x tagging method, largely improving these shortcomings. It includes the main chemical reactions of HO_x chemistry in the troposphere and stratosphere. This is enabled by introducing the tagging of the hydrogen radical (H). Special care is taken for the steady-state assumption.

The paper is structured as follows: after introducing the model set-up in Sect. 2, we present the advanced HO_x tagging method V1.1 in Sect. 3. In Sect. 4, the results are compared with the tagging method V1.0 by Grewe et al. (2017). Finally, Sect. 5 concludes the methods and the results of this study.

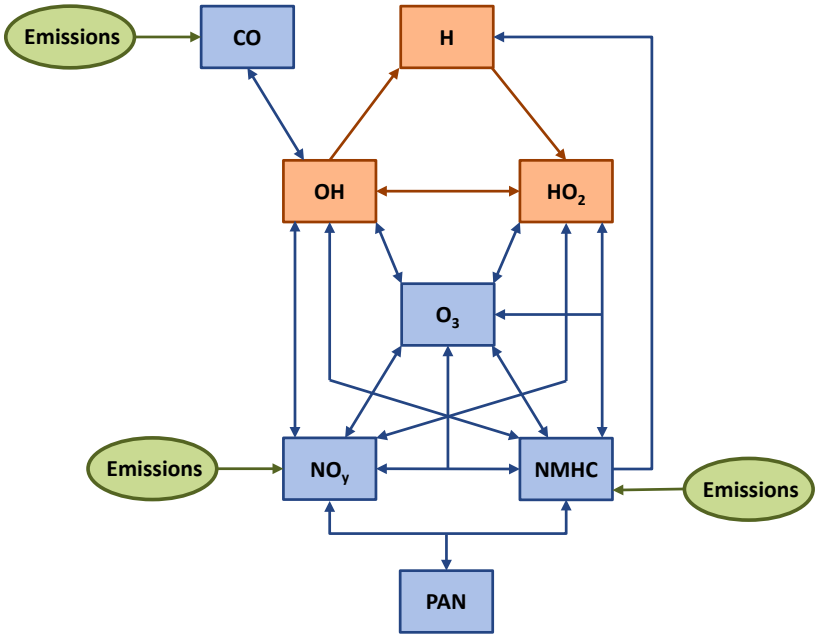

Figure 1. Sketch of the chemistry used in advanced tagging mechanism V1.1. Blue boxes indicate tagged long-lived species, and orange boxes display tagged short-lived species. Green boxes represent the emissions of CO, NO_y and NMHC.

2 Model description of EMAC and MECO(n)

To evaluate the further developed HO_x tagging method we use the same model set-up as Grewe et al. (2017). A global climate simulation is performed with the ECHAM/MESSy Atmospheric Chemistry (EMAC) chemistry climate model. EMAC is a numerical chemistry and climate simulation system that includes submodels describing tropospheric and middle atmosphere processes and their interaction with oceans, land and human influences (Jöckel et al., 2010). It uses the second version of the Modular Earth Submodel System (MESSy2.53) to link multi-institutional computer codes. The core atmospheric model is the 5th generation European Centre Hamburg general circulation model (ECHAM5; Roeckner et al., 2006). For the present study we apply EMAC in the T42L90MA resolution, i.e. with a spherical truncation of T42 (corresponding to a quadratic Gaussian grid of approx. 2.8 by 2.8° in latitude and longitude) with 90 vertical hybrid pressure levels up to 0.01 hPa. For the simulation presented in this study, the time span of July 2007 to December 2008 is considered: half a year as a spin-up and 1 year for the analysis.

For the chemical scheme, we use the submodel MECCA (Module Efficiently Calculating the Chemistry of the Atmosphere), which is based on Sander et al. (2011) and Jöckel et al. (2010). The chemical mechanism includes 218 gas-phase, 12 heterogeneous and 68 photolysis reactions. In total 188 species are considered. It regards the basic chemistry of OH, HO_2, O_3, CH_4, nitrogen oxides, alkanes, alkenes, chlorine and bromine. Alkynes, aromatics and mercury are not considered.

Total global emissions of lightning NO_x are scaled to approximately 4 Tg(N) a^{-1} (parameterized according to Grewe et al., 2001). The submodel ONEMIS (Kerkweg et al., 2006) calculates NO_x emissions from soil (parameterized according to Yienger and Levy, 1995) and biogenic C_5H_8 emissions (parameterized according to Guenther et al., 1995). Direct CH_4 emissions are not considered, and instead pseudo-emissions are calculated using the submodel TNUDGE (Kerkweg et al., 2006). This submodel relaxes the mixing ratios in the lowest model layer towards observations by Newtonian relaxation (more details are given by Jöckel et al., 2016).

To show the effect of the HO_x tagging method on a regional scale, a further simulation with the coupled model system MESSyfied ECHAM and COSMO models nested n times (MECO(n)) is performed. The nested system couples the global chemistry climate model EMAC online with the regional chemistry climate model COSMO/MESSy (Kerkweg and Jöckel, 2012a, b). To test the HO_x tagging in MECO(n), we conduct a simulation using one COSMO/MESSy nest over Europe with a resolution of 0.44°. EMAC is applied in a horizontal resolution of T42 with 31 vertical levels. The period from July 2007 to December 2008 is simulated. The set-up of the simulation is identical to the one described in Grewe et al. (2017). A detailed chemical evaluation of the set-up is given in Mertens et al. (2016).

Both model simulations are based on the quasi chemistry-transport model (QCTM) mode in which the chemistry is decoupled from the dynamics (Deckert et al., 2011). The anthropogenic emissions are taken from the MACCity emission inventory (Granier et al., 2011). The TAGGING submodel (as described by Grewe et al., 2017) is coupled to the detailed chemical solver MECCA from which it obtains information about tracer concentrations and reaction rates. Based on this information, it calculates the contributions of source categories to O_3, CO, NO_y, PAN and NMHC concentrations. The contributions of OH and HO_2 are calculated with the advanced method V1.1 presented in the next section. The implementation is based on MESSy2.53 and will be available in MESSy2.54.

3 Tagging method of short-lived species

3.1 Tagging method V1.0

The tagging method V1.0 described by Grewe et al. (2017) determines the contribution of source categories to O_3, NO_y, CO, NMHC, PAN, OH and HO_2 concentrations. A total of 10 source categories are considered, and every species included in the tagging method is decomposed into these categories: for example, the concentration of O_3 is split up into O_3 produced by anthropogenic non-traffic (e.g. industry) emissions (O_3^{ant}), road traffic emissions (O_3^{tra}), ship emissions (O_3^{shp}), air traffic emissions (O_3^{air}), biogenic emissions (O_3^{bio}), biomass burning (O_3^{bb}), lightning (O_3^{lig}), methane decomposition ($O_3^{CH_4}$), nitrous oxide decomposition ($O_3^{N_2O}$) and stratospheric ozone production (O_3^{str}). These tagged species go through the same chemical reactions and the same deposition loss processes as O_3. The tagging method uses a combinatoric approach to determine the contributions: it redistributes the production and loss rates of each species to the 10 source categories according to the concentrations of the tagged species. Details on the tagging theory and implementation in EMAC and MECO(n) are found in Grewe (2013) and Grewe et al. (2017), respectively.

For the first time, V1.0 determined the contribution of source categories to OH and HO_2 concentrations. The tagging method V1.0 was based on 12 reactions for the HO_x chemistry (reactions marked with "o" in last column of Table 1). It included the main production and loss reactions of HO_x with O_3, NO_y, NMHC, CO and CH_4. V1.0 only regarded reactions which are important in the troposphere. Reactions which mainly occur in the stratosphere were not taken into account. However, the main HO_2 production by the Reaction (1) $H + O_2 \longrightarrow HO_2$ (see Table 1) was not regarded. It was combined with Reaction (11), $CO + OH \longrightarrow H + CO_2$ (see Table 1), to

$$\begin{aligned} &CO + OH \longrightarrow CO_2 + H \\ &\qquad \xrightarrow{O_2} CO_2 + HO_2 \\ \Longrightarrow\ &CO + OH \xrightarrow{O_2} CO_2 + HO_2. \end{aligned}$$

But not all H radicals in the troposphere are produced by the reaction of $CO + OH$. Reactions (7) $OH + O(^3P)$, (10) $H_2 + OH$ and (28) $HCHO + h\nu$ also produce H (Table 2). These reactions were neglected in V1.0. Thus, only 80 % of the H production and therefore only 80 % of the HO_2 production by Reaction (1) was considered in the troposphere. In the stratosphere, the reaction of $CO + OH$ becomes less important and most H is produced by Reactions (7) and (28). Consequently, only 6 % of the H and thus of the HO_2 production by Reaction (1) was regarded in this approach. (Numbers are derived from an EMAC simulation as described in Sect. 2.)

In the troposphere, the most important reactions not covered in V1.0 are Reaction (1) $H + O_2$, Reaction (15) $NO_2 + HO_2$ and Reaction (18) for the decomposition of HNO_4. In the stratosphere, Reactions (1) $H + O_2$, (5) $HO_2 + O(^3P)$ and (7) $OH + O(^3P)$ play a leading role and were not included in V1.0.

Most reaction rates used in the tagging method correspond to the production and loss rates directly provided by the chemical scheme MECCA of EMAC. However, for reactions with NMHC, the reaction rates were obtained indirectly. The reaction rate of OH with NMHC (Reaction 21, Table 1) was determined via the production rates of CO by assuming that each reaction of OH with NMHC produces one CO molecule. This method neglects all intermediate oxidation reactions of NMHC and considers only these reactions when NMHC is finally oxidized to CO. For the reaction rates of NO_y and HO_2 with NMHC (Reactions 22 and 23), only the reaction of HO_2 with the methylperoxy radical (CH_3O_2) was considered.

To derive the contributions to OH and HO_2, a steady state between HO_x production and loss was assumed. However, the steady-state assumption was not completely fulfilled for V1.0 (see Sect. 3.4). Moreover, the sum of the contributions of the 10 source categories to the OH and HO_2 concentrations did not equal the total OH and HO_2 concentrations. It deviated by about 70 %.

3.2 Reduced HO_x reaction system V1.1

OH and HO_2 react with many chemical species. To reduce the calculation time of a simulation, we reduce the HO_x chemistry used in the chemical scheme MECCA to the most important reactions which occur in the troposphere and stratosphere. We consider only reactions with a tropospheric or stratospheric annual mean reaction rate larger than 10^{-15} mol mol^{-1} s^{-1} (see Table 1). Hence, we increase the number of reactions from 12 (V1.0) to 27 (V1.1), which still constitutes a reduced set of reactions compared to the full chemical scheme MECCA used in EMAC. In the following, we call this set *reduced HO_x reaction system V1.1*.

The reactions which are important in the troposphere are indicated in Table 1. As stated above, Reaction (1) of H and

Table 1. The reduced HO_x reaction system V1.1 describes the main reactions of HO_x chemistry in the troposphere and stratosphere. These 27 reactions are used for the tagging method V1.1. In the column "tropos." ("stratos."), reactions which are important in the troposphere (stratosphere) are marked. In the column "V1.1", reactions marked with "o" were already included in V1.0. Reactions marked with "x" are added in V1.1. Reactions marked with "(x)" were only partly taken into account in V1.0. The numbers of reactions are referenced in the text.

	Reaction			Rates	Tropos.	Stratos.	V1.1
1	$H + O_2$	$\longrightarrow$	HO_2	R_1	x	x	(x)
2	$H_2O + O(^1D)$	$\longrightarrow$	2 OH	R_2	x	x	o
3	$HO_2 + HO_2$	$\longrightarrow$	$H_2O_2 + O_2$	R_3	x		o
4	$HO_2 + O_3$	$\longrightarrow$	$OH + 2\,O_2$	R_4	x	x	o
5	$HO_2 + O(^3P)$	$\longrightarrow$	$OH + O_2$	R_5		x	x
6	$OH + O_3$	$\longrightarrow$	$HO_2 + O_2$	R_6	x	x	o
7	$OH + O(^3P)$	$\longrightarrow$	$H + O_2$	R_7		x	x
8	$HO_2 + OH$	$\longrightarrow$	$H_2O + O_2$	R_8	x	x	o
9	$H_2O_2 + OH$	$\longrightarrow$	$H_2O + HO_2$	R_9	x		x
10	$H_2 + OH$	$\longrightarrow$	$H_2O + H$	R_{10}	x		x
11	$CO + OH$	$\longrightarrow$	$H + CO_2$	R_{11}	x	x	o
12	$CH_4 + OH$	$\longrightarrow$	$CH_3 + H_2O$	R_{12}	x	x	o
13	$ClO + OH$	$\longrightarrow$	$0.94\,Cl + 0.94\,HO_2 + 0.06\,HCl + 0.06\,O_2$	R_{13}		x	x
14	$NO + HO_2$	$\longrightarrow$	$NO_2 + OH$	R_{14}	x	x	o
15	$NO_2 + HO_2$	$\longrightarrow$	HNO_4	R_{15}	x	x	x
16	$NO + OH$	$\longrightarrow$	$HONO$	R_{16}		x	x
17	$NO_2 + OH$	$\longrightarrow$	HNO_3	R_{17}		x	o
18	HNO_4	$\longrightarrow$	$NO_2 + HO_2$	R_{18}	x		x
19	$HONO + h\nu$	$\longrightarrow$	$NO + OH$	R_{19}		x	x
20	$HNO_3 + h\nu$	$\longrightarrow$	$NO_2 + OH$	R_{20}		x	x
21	$NMHC + OH$	$\longrightarrow$	NMHC	R_{21}	x		o
22	$NMHC + HO_2$	$\longrightarrow$	NMHC	R_{22}	x		o
23	$NMHC + NO_y$	$\longrightarrow$	$HO_2 + NMHC + NO_y$	R_{23}	x	x	o
24	$NMHC + OH$	$\longrightarrow$	$NMHC + HO_2$	R_{24}	x		x
25	$NMHC + h\nu$	$\longrightarrow$	$NMHC + HO_2$	R_{25}	x		x
26	$ClO + HO_2$	$\longrightarrow$	$HOCl + O_2$	R_{26}		x	x
27	$BrO + HO_2$	$\longrightarrow$	$HOBr + O_2$	R_{27}		x	x

Table 2. The reduced H reaction system describes the main reactions of H. In the column "tropos." ("stratos."), reactions which are important in the troposphere (stratosphere) are marked. The numbers of the reactions correspond to the numbers in Table 1.

	Reaction			Rates	Tropos.	Stratos.
1	$H + O_2$	$\longrightarrow$	HO_2	R_1	x	x
7	$OH + O(^3P)$	$\longrightarrow$	$H + O_2$	R_7		x
10	$H_2 + OH$	$\longrightarrow$	$H_2O + H$	R_{10}	x	
11	$CO + OH$	$\longrightarrow$	$H + CO_2$	R_{11}	x	x
28	$HCHO + O_2 + h\nu$	$\longrightarrow$	$H + CO + HO_2$	R_{28}	x	

O_2 dominates the HO_2 production in the troposphere. It produces 49 % of tropospheric HO_2. In V1.0, only part of this HO_2 source was regarded (see Sect. 3.1). The most important HO_2 loss is the reaction with NO (Reaction 14), followed by the reaction with itself producing H_2O_2 (Reaction 3), which accounts for 32 and 12 % of tropospheric HO_2 loss. The production via H_2O and $O(^1D)$ produces about 21 % of tropospheric OH (Reaction 2). The excited oxygen radical ($O(^1D)$) originates from the photolysis of O_3. Reaction (14) of NO and HO_2 also produces 32 % of tropospheric OH. OH is mostly destroyed by CO (Reaction 11, 38 %), followed by NMHC (Reaction 21, 25 %).

In the stratosphere different chemical reactions become important. Here, OH is mainly destroyed by O_3, producing 40 % of stratospheric HO_2. The reaction is partly counteracted by the Reaction (14), which produces 21 % of OH and destroys 24 % of HO_2. Since large quantities of O_3 are found in the stratosphere, O_3 or the excited oxygen radical ($O(^3P)$) destroys about 62 % of HO_2. Reactions with NMHC, CO and CH_4 play only a minor role in the stratosphere.

Reactions of OH and HO_2 with chlorine and bromide were not considered in V1.0. We add these reactions, which take place only in the stratosphere, to the tagging method V1.1. Reactions (21) to (25) involve the chemical family NMHC, which contains several species such as formaldehyde (HCHO), ethylene (C_2H_4) and propane (C_3H_8). The rate for Reaction (21) is determined by adding up the rates of all reactions of OH with each single species of the family NMHC. The reaction rate (23) contains all rates of the reactions between the species of the chemical families NO_y and NMHC. All reaction rates are directly derived by the MECCA mechanism of EMAC.

Table 1 does not consider all reactions with annual reaction rates larger than 10^{-15} mol mol^{-1} s^{-1}. The photolysis of hydrogen peroxide (H_2O_2), hypochlorous acid (HOCl) and hypobromous acid (HOBr) is excluded from the reduced HO_x reaction system V1.1 as the tagging method cannot be applied. The specific reasons are explained in Appendix A.

3.3 Deductions of tagged species

To derive how much OH and HO_2 is produced and destroyed by a source category i, the tagging approach described in Grewe et al. (2010); Grewe et al. (2017) is used. In general, bimolecular reactions with two chemical species $A + B \longrightarrow C$ are tagged as follows: each tagged species is split up into its contribution from n source categories $A = \sum_{i=1}^{n} A^i$, $B = \sum_{i=1}^{n} B^i$ and $C = \sum_{i=1}^{n} C^i$. These contributions (A^i, B^i, C^i) go through the same reactions as their main species (A, B, C). If A from category i reacts with B from category j, then the resulting species C belongs half to the category i and half to the category j:

$$A^i + B^j \longrightarrow \frac{1}{2}C^i + \frac{1}{2}C^j. \tag{1}$$

Consequently, the production P and loss L of a species from the category i (here LossA^i, LossB^i and ProdC^i) are determined by regarding all possible combinations of the reaction between A^i and B^j:

$$\begin{aligned}\mathrm{LossA}^i &= \mathrm{LossB}^i = \mathrm{ProdC}^i \\ &= k\left(A^i B^i + \sum_{j=1, j\neq i}^{n} \frac{1}{2}A^i B^j + \sum_{j=1, j\neq i}^{n} \frac{1}{2}A^j B^i\right) \\ &= \frac{1}{2}R\left(\frac{A^i}{A} + \frac{B^i}{B}\right),\end{aligned} \tag{2}$$

with k being the reaction rate coefficient and $R = k\ A\ B$ being the respective reaction rate. For unimolecular reactions $A \longrightarrow B + C$, the distribution of categories from the educts is completely passed to the products:

$$\mathrm{LossA}^i = \mathrm{ProdB}^i = \mathrm{ProdC}^i = R\frac{A^i}{A}, \tag{3}$$

with the reaction rate $R = kA$.

As described above, the long-lived species O_3, CO, NO_y and NMHC are tagged according to the tagging method described in Grewe et al. (2017). To limit memory demand, other species such as H_2, H_2O_2, CH_4, ClO and BrO are not tagged (as in V1.0). Here, different approaches are derived to retain the ratio of the contribution to total concentration $\frac{A^i}{A}$.

1. If a tagged species reacts with a non-tagged species, the non-tagged species does not contribute and the tagging method for a unimolecular reaction is applied (see Eq. 3). Examples are Reactions (9), (10) and (13).

2. Using the family concept as described in Grewe et al. (2017) allows for the assumption that all tags are distributed equally among the species within the same chemical family.

$$\frac{\mathrm{NO}^i}{\mathrm{NO}} = \frac{\mathrm{NO_2}^i}{\mathrm{NO_2}} = \frac{\mathrm{HNO_4}^i}{\mathrm{HNO_4}} = \frac{\mathrm{NO}_y^i}{\mathrm{NO}_y} \tag{4}$$

   As mentioned in Grewe et al. (2017), all species which are frequently converted back and forth to ozone are considered as an "ozone storage" (Crutzen and Schmailzl, 1983). These species together with O_3 are lumped into one chemical family: ozone. Both $O(^1D)$ and $O(^3P)$ belong to this chemical family. Hence, as in Grewe et al. (2017), we apply the family concept and set

$$\frac{\mathrm{O}(^1\mathrm{D})^i}{\mathrm{O}(^1\mathrm{D})} = \frac{\mathrm{O}(^3\mathrm{P})^i}{\mathrm{O}(^3\mathrm{P})} = \frac{\mathrm{O_3}^i}{\mathrm{O_3}}. \tag{5}$$

3. In Reaction (1), neither H nor O_2 is tagged. To obtain the ratio $\frac{\mathrm{HO_2}^i}{\mathrm{HO_2}}$, we set up an extra tagging of H itself. As the H radical is very reactive, we assume that H production balances H loss (see Sect. 3.4). Table 2 presents the main reactions for H, which still constitute a subset of full H chemistry implemented in MECCA. Based on Table 2, we set up the H production ProdH^i and H loss LossH^i for the contribution of a source category i.

$$\begin{aligned}\mathrm{ProdH}^i = &\frac{1}{2}R_7\left(\frac{\mathrm{OH}^i}{\mathrm{OH}} + \frac{\mathrm{O_3}^i}{\mathrm{O_3}}\right) + R_{10}\frac{\mathrm{OH}^i}{\mathrm{OH}} \\ &+ \frac{1}{2}R_{11}\left(\frac{\mathrm{CO}^i}{\mathrm{CO}} + \frac{\mathrm{OH}^i}{\mathrm{OH}}\right) + R_{28}\frac{\mathrm{NMHC}^i}{\mathrm{NMHC}}\end{aligned} \tag{6}$$

$$\mathrm{LossH}^i = R_1\frac{\mathrm{H}^\mathrm{i}}{\mathrm{H}} \tag{7}$$

   As mentioned above, the family concept also sets $\frac{\mathrm{HCHO}^i}{\mathrm{HCHO}} = \frac{\mathrm{NMHC}^i}{\mathrm{NMHC}}$. Since the steady-state assumption applies for H (see Sect. 3.4), the H production per source

Table 3. Annual mean of OH, HO_2 and H production and loss rates (air mass weighted) in 10^{-13} mol mol^{-1} s^{-1} for the total rates (derived from the complete chemical scheme MECCA in EMAC) and for the rates of the reduced reaction system of the tagging method V1.0 and V1.1. The first row gives the rates for the troposphere, and the second row for the stratosphere (written in italic).

		OH		HO_2		H	
		Prod.	Loss	Prod.	Loss	Prod.	Loss
Total – MECCA	tropos.	0.49	0.49	0.49	0.49	0.24	0.24
	stratos.	*2.78*	*2.78*	*2.48*	*2.48*	*7.09*	*7.09*
Reduced – V1.1	tropos.	0.43	0.48	0.47	0.49	0.24	0.24
	stratos.	*2.49*	*2.76*	*2.47*	*2.48*	*7.06*	*5.99*
Reduced – V1.0	tropos.	0.43	0.47	0.29	0.42	–	–
	stratos.	*0.86*	*1.30*	*1.19*	*0.84*	–	–

category i ProdH^i equals the loss LossH^i. After setting Eqs. (6) and (7) equal to each other, we obtain

$$\frac{H^i}{H} = \frac{1}{2}\frac{R_7}{R_1}\left(\frac{OH^i}{OH} + \frac{{O_3}^i}{O_3}\right) + \frac{R_{10}}{R_1}\frac{OH^i}{OH} + \frac{1}{2}\frac{R_{11}}{R_1}\left(\frac{CO^i}{CO} + \frac{OH^i}{OH}\right) + \frac{R_{28}}{R_1}\frac{NMHC^i}{NMHC}. \quad (8)$$

These different approaches are applied to the reduced HO_x reaction system V1.1 (Table 1) to derive the contributions of source categories to OH and HO_2 in Sect. 3.5.

3.4 Steady-state assumption

The steady-state assumption of the HO_x chemistry is the basic principle of the tagging method for short-lived species (Tsati, 2014; Grewe et al., 2017). In steady state, the production and loss of OH and HO_2 balance each other. Table 3 shows the annual means of the HO_x and H production and loss rates of the reduced reaction system for the tagging methods V1.0 and V1.1 as well as the total production and loss rates derived from the complete chemical scheme MECCA in EMAC. The production and loss rates are obtained from an EMAC simulation following the set-up described in Sect. 2. Note that for V1.0 no values for the H production and loss are available since the tagging of H was not considered in V1.0.

In general, total OH production (derived by MECCA) equals total OH loss in the troposphere and stratosphere. The same holds for HO_2 and H. In the troposphere, the OH loss of V1.1 and V1.0 represents the total OH loss in the troposphere well. However, the OH production for V1.1 and V1.0 differs by 12 % from the total OH production. Considering HO_2 in the troposphere, the total production and loss rates are well reflected by V1.1. In contrast, the HO_2 production and loss of V1.0 differs by 14 and 41 % from the total rates.

In the stratosphere, V1.1 represents the total rates very well. However, the OH production of V1.1 misses 10 % of the total OH production. Since V1.0 was only developed for the troposphere, not all reactions which are important in the stratosphere were considered. Thus, the OH and HO_2 production and loss rates of V1.0 considerably underestimated the total production and loss rates.

The reduced H reaction system in V1.1 (Table 2) represents the total H production and loss in the troposphere very well. However, in the stratosphere H loss in V1.1 deviates by 17 % from the total H loss.

Summing up, the reduced HO_x reaction system V1.1 represents the total HO_x production and loss in the troposphere and stratosphere well. V1.1 reproduces the HO_x chemistry better than V1.0. However, OH production in the troposphere and stratosphere as well as H loss in the stratosphere of V1.1 deviate from the total rates derived by MECCA. Thus, the steady state for the reduced HO_x and H reaction system (Tables 1 and 2) is not completely fulfilled.

But steady state between production and loss is crucial for the tagging method for short-lived species. To re-establish steady state, it would be necessary to include the complete HO_x and H chemistry in the tagging method. However, this is not possible as the tagging method of short-lived species does not apply to all reactions of the HO_x and H chemistry (for examples see Appendix A). Moreover, tagging all chemical species of the HO_x and H chemistry with the implementation of long-lived species would significantly increase the memory demand of a climate simulation (for a detailed discussion see Sect. 6 in Grewe et al., 2017). Consequently, we introduce the rest terms resOH, resHO_2 and resH for OH, HO_2 and H to compensate for the deviations from steady state. Each rest term is calculated by subtracting the production rate of the reduced reaction system from the loss rate (Tables 1 and 2). The resulting rest terms are shown in the Supplement (Fig. S1).

Considering the rest terms resOH, resHO_2 and resH leads to the closure of the budget. In V1.0, the sum of the contributions from all source categories did not balance the total concentration. The averaged deviations for OH and HO_2 in the troposphere were about 70 % of the total concentrations. Since the stratosphere was not considered in V1.0, the deviations were even larger (104 % for OH and 89 % for HO_2). In V1.1, the sum of OH and HO_2 now balances the total OH

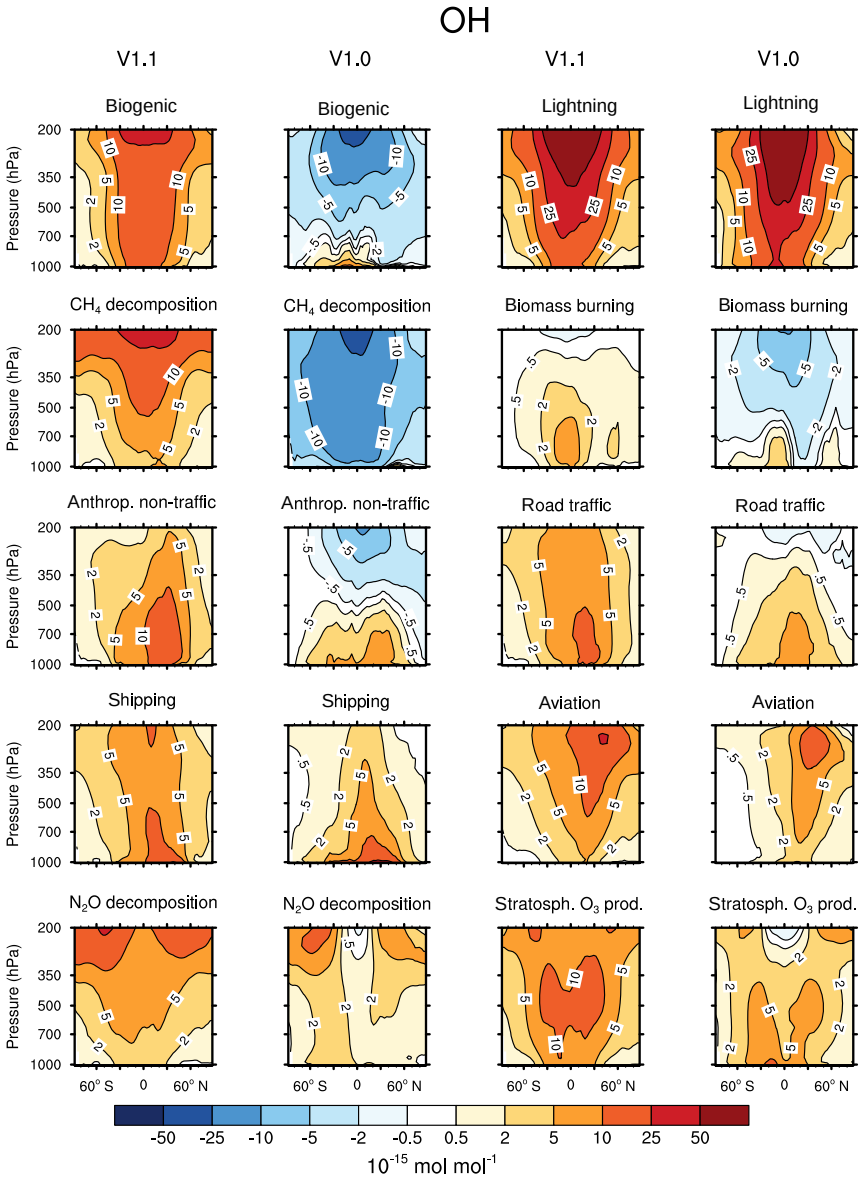

Figure 2. Contribution of 10 source categories to OH in 10^{-15} mol mol^{-1}. Zonal means of the year 2008 are shown. First and third columns show the tagging method V1.1. Second and forth columns show the tagging method V1.0. Simulation is performed with EMAC.

and HO_2 concentrations. The deviations are negligible (below 10^{-3} %). Consequently, including the rest terms in the tagging method is mandatory for the steady-state assumption and also closes the budget.

3.5 Determination of HO_x contributions

Taking the above considerations into account, we finally derive the OH and HO_2 production and loss terms per source category i. In the reduced HO_x reaction system V1.1 (Table 1), OH is produced by the Reactions (2) $H_2O + O(^1D)$, (4) $HO_2 + O_3$, (5) $HO_2 + O(^3P)$, (14) $NO + HO_2$, (19) $HONO + h\nu$ and (20) $HNO_3 + h\nu$. Applying the partitioning described in Sect. 3.3, the OH production for a source category i ProdOH^i is determined as follows.

$$\mathrm{ProdOH}^i = 2 \cdot R_2 \frac{{O_3}^i}{O_3} + \frac{1}{2} R_4 \left(\frac{{HO_2}^i}{HO_2} + \frac{{O_3}^i}{O_3} \right) + \frac{1}{2} R_5 \left(\frac{{HO_2}^i}{HO_2} + \frac{{O_3}^i}{O_3} \right) + \frac{1}{2} R_{14} \left(\frac{{NO_y}^i}{NO_y} + \frac{{HO_2}^i}{HO_2} \right)$$

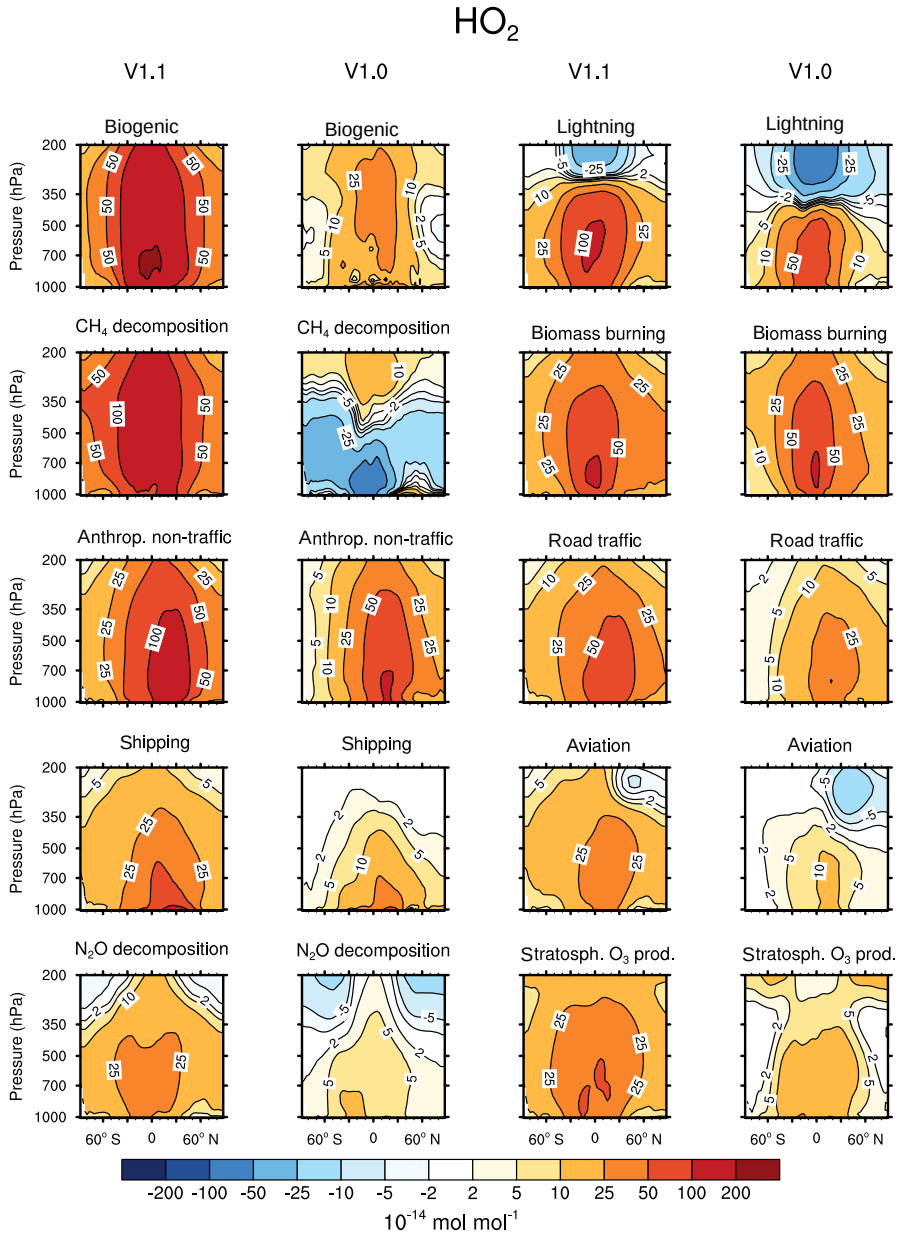

Figure 3. Contribution of 10 source categories to HO_2 in 10^{-14} mol mol^{-1}. Zonal means of the year 2008 are shown. First and third columns show the tagging method V1.1. Second and forth columns show the tagging method V1.0. Simulation is performed with EMAC.

$$+ R_{19}\frac{NO_y^i}{NO_y} + R_{20}\frac{NO_y^i}{NO_y} \tag{9}$$

OH is destroyed by the Reactions (6) $OH + O_3$, (7) $OH + O(^3P)$, (8) $HO_2 + OH$, (9) $H_2O_2 + H$, (10) $H_2 + OH$, (11) $CO + OH$, (12) $CH_4 + OH$, (13) $ClO + OH$, (16) $NO + OH$, (17) $NO_2 + OH$, (21) $NMHC + OH$ and (24) $NMHC + OH$. The OH loss per source category i $LossOH^i$ is

$$\begin{aligned}
LossOH^i = {} & \frac{1}{2}R_6\left(\frac{OH^i}{OH} + \frac{{O_3}^i}{O_3}\right) + \frac{1}{2}R_7\left(\frac{OH^i}{OH} + \frac{{O_3}^i}{O_3}\right) \\
& + \frac{1}{2}R_8\left(\frac{{HO_2}^i}{HO_2} + \frac{OH^i}{OH}\right) + \frac{1}{2}R_9\left(\frac{{HO_2}^i}{HO_2} + \frac{OH^i}{OH}\right) \\
& + R_{10}\frac{OH^i}{OH} + \frac{1}{2}R_{11}\left(\frac{CO^i}{CO} + \frac{OH^i}{OH}\right) + R_{12}\frac{OH^i}{OH} \\
& + R_{13}\frac{OH^i}{OH} + \frac{1}{2}R_{16}\left(\frac{NO_y^i}{NO_y} + \frac{OH^i}{OH}\right) \\
& + \frac{1}{2}R_{17}\left(\frac{NO_y^i}{NO_y} + \frac{OH^i}{OH}\right)
\end{aligned}$$

$$+\frac{1}{2}R_{21}\left(\frac{\mathrm{NMHC}^i}{\mathrm{NMHC}}+\frac{\mathrm{OH}^i}{\mathrm{OH}}\right)$$
$$+\frac{1}{2}R_{24}\left(\frac{\mathrm{NMHC}^i}{\mathrm{NMHC}}+\frac{\mathrm{OH}^i}{\mathrm{OH}}\right). \quad (10)$$

HO_2 is produced by Reactions (1) $H+O_2$, (6) OH+, O_3, (9) H_2O_2+OH, (13) $ClO+OH$, (18) HNO_4, (23) $NMHC+NO_y$, (24) $NMHC+OH$ and (25) $NMHC+h\nu$. However, H in Reaction (1) is not tagged. To be able to determine the HO_2 production by Reaction (1) $R_1\frac{\mathrm{H}^i}{\mathrm{H}}$, we apply the introduced H tagging (see Sect. 3.3) and replace $\frac{\mathrm{H}^i}{\mathrm{H}}$ with Eq. (8). In addition, Reaction (13) constitutes a simplified reaction producing $0.94\cdot HO_2$. Consequently, the HO_2 production per source category i ProdHO2^i is

$$\begin{aligned}\mathrm{ProdHO}_2^i = {}&\frac{1}{2}R_6\left(\frac{\mathrm{OH}^i}{\mathrm{OH}}+\frac{{\mathrm{O}_3}^i}{\mathrm{O}_3}\right)+\frac{1}{2}R_7\left(\frac{\mathrm{OH}^i}{\mathrm{OH}}+\frac{{\mathrm{O}_3}^i}{\mathrm{O}_3}\right)\\&+\frac{1}{2}R_9\left(\frac{{\mathrm{HO}_2}^i}{\mathrm{HO}_2}+\frac{\mathrm{OH}^i}{\mathrm{OH}}\right)+R_{10}\frac{\mathrm{OH}^i}{\mathrm{OH}}\\&+\frac{1}{2}R_{11}\left(\frac{\mathrm{CO}^i}{\mathrm{CO}}+\frac{\mathrm{OH}^i}{\mathrm{OH}}\right)+0.94\cdot R_{13}\frac{\mathrm{OH}^i}{\mathrm{OH}}\\&+R_{18}\frac{\mathrm{NO}_y^i}{\mathrm{NO}_y}+\frac{1}{2}R_{23}\left(\frac{\mathrm{NMHC}^i}{\mathrm{NMHC}}+\frac{\mathrm{NO}_y^i}{\mathrm{NO}_y}\right)\\&+\frac{1}{2}R_{24}\left(\frac{\mathrm{NMHC}^i}{\mathrm{NMHC}}+\frac{\mathrm{OH}^i}{\mathrm{OH}}\right)+R_{25}\frac{\mathrm{NMHC}^i}{\mathrm{NMHC}}\\&+R_{28}\frac{\mathrm{NMHC}^i}{\mathrm{NMHC}}. \quad (11)\end{aligned}$$

The HO_2 loss is determined by Reactions (3) HO_2+HO_2, (4) HO_2+O_3, (5) $HO_2+O(^3P)$, (8) HO_2+OH, (14) $NO+HO_2$, (15) NO_2+HO_2, (22) $NMHC+HO_2$, (26) $ClO+HO_2$ and (27) $BrO+HO_2$. Hence, the HO_2 loss per source category i LossHO2^i is

$$\begin{aligned}\mathrm{LossHO}_2^i = {}&R_3\frac{{\mathrm{HO}_2}^i}{\mathrm{HO}_2}+\frac{1}{2}R_4\left(\frac{{\mathrm{HO}_2}^i}{\mathrm{HO}_2}+\frac{{\mathrm{O}_3}^i}{\mathrm{O}_3}\right)\\&+\frac{1}{2}R_5\left(\frac{{\mathrm{HO}_2}^i}{\mathrm{HO}_2}+\frac{{\mathrm{O}_3}^i}{\mathrm{O}_3}\right)+\frac{1}{2}R_8\left(\frac{{\mathrm{HO}_2}^i}{\mathrm{HO}_2}+\frac{\mathrm{OH}^i}{\mathrm{OH}}\right)\\&+\frac{1}{2}R_{14}\left(\frac{\mathrm{NO}_y^i}{\mathrm{NO}_y}+\frac{{\mathrm{HO}_2}^i}{\mathrm{HO}_2}\right)\\&+\frac{1}{2}R_{15}\left(\frac{\mathrm{NO}_y^i}{\mathrm{NO}_y}+\frac{{\mathrm{HO}_2}^i}{\mathrm{HO}_2}\right)\\&+\frac{1}{2}R_{22}\left(\frac{\mathrm{NMHC}^i}{\mathrm{NMHC}}+\frac{{\mathrm{HO}_2}^i}{\mathrm{HO}_2}\right)+R_{26}\frac{{\mathrm{HO}_2}^i}{\mathrm{HO}_2}\\&+R_{27}\frac{{\mathrm{HO}_2}^i}{\mathrm{HO}_2}. \quad (12)\end{aligned}$$

Section 3.4 shows that the steady-state assumption for OH and HO_2 is justified when the rest terms resOH, resHO$_2$ and resH are regarded. Therefore, the rest terms are divided by the number of source categories n to add them to the contributions of a category i. In steady state, production of OH^i and HO$_2{}^i$ equals the loss.

$$\mathrm{ProdOH}^i-\mathrm{LossOH}^i+\mathrm{resOH}/n=0 \quad (13)$$
$$\mathrm{ProdHO}_2^i-\mathrm{LossHO}_2^i+\mathrm{resHO}_2/n+\mathrm{resH}/n=0 \quad (14)$$

Equations (13) and (14) are rewritten as follows:

$$0=A^i-L^{\mathrm{OH}}\frac{\mathrm{OH}^i}{\mathrm{OH}}+P^{\mathrm{OH}}\frac{\mathrm{HO}_2^i}{\mathrm{HO}_2}+\frac{\mathrm{resOH}}{n}, \quad (15)$$
$$0=B^i+P^{\mathrm{HO}_2}\frac{\mathrm{OH}^i}{\mathrm{OH}}-L^{\mathrm{HO}_2}\frac{{\mathrm{HO}_2}^i}{\mathrm{HO}_2}+\frac{\mathrm{resHO}_2}{n}+\frac{\mathrm{resH}}{n}, \quad (16)$$

with the variables P^{OH}, L^{OH}, P^{HO_2}, L^{HO_2}, A^i and B^i as follows (compare to Grewe et al., 2017 Eqs. 25 to 28).

$$P^{\mathrm{OH}}=\frac{1}{2}R_4+\frac{1}{2}R_5+\frac{1}{2}R_{14}-\frac{1}{2}R_8 \quad (17)$$

$$\begin{aligned}L^{\mathrm{OH}} = {}&\frac{1}{2}R_6+\frac{1}{2}R_7+\frac{1}{2}R_8+R_9+R_{10}+\frac{1}{2}R_{11}\\&+R_{12}+R_{13}+\frac{1}{2}R_{16}+\frac{1}{2}R_{17}+\frac{1}{2}R_{21}+\frac{1}{2}R_{24} \quad (18)\end{aligned}$$

$$\begin{aligned}P^{\mathrm{HO}_2} = {}&\frac{1}{2}R_6+\frac{1}{2}R_7+R_9+R_{10}+\frac{1}{2}R_{11}\\&+0.94\cdot R_{13}+\frac{1}{2}R_{24}-\frac{1}{2}R_8 \quad (19)\end{aligned}$$

$$\begin{aligned}L^{\mathrm{HO}_2} = {}&2\cdot R_3+\frac{1}{2}R_4+\frac{1}{2}R_5+\frac{1}{2}R_8+\frac{1}{2}R_{14}+\frac{1}{2}R_{15}\\&+\frac{1}{2}R_{22}+R_{26}+R_{27} \quad (20)\end{aligned}$$

$$\begin{aligned}A^i = {}&2\cdot R_2\frac{{\mathrm{O}_3}^i}{\mathrm{O}_3}+\frac{1}{2}R_4\frac{{\mathrm{O}_3}^i}{\mathrm{O}_3}+\frac{1}{2}R_5\frac{{\mathrm{O}_3}^i}{\mathrm{O}_3}+\frac{1}{2}R_{14}\frac{\mathrm{NO}_y^i}{\mathrm{NO}_y}\\&+R_{19}\frac{\mathrm{NO}_y^i}{\mathrm{NO}_y}+R_{20}\frac{\mathrm{NO}_y^i}{\mathrm{NO}_y}-\frac{1}{2}R_6\frac{{\mathrm{O}_3}^i}{\mathrm{O}_3}\\&-\frac{1}{2}R_7\frac{{\mathrm{O}_3}^i}{\mathrm{O}_3}-\frac{1}{2}R_{11}\frac{\mathrm{CO}^i}{\mathrm{CO}}-\frac{1}{2}R_{16}\frac{\mathrm{NO}_y^i}{\mathrm{NO}_y}\\&-\frac{1}{2}R_{17}\frac{\mathrm{NO}_y^i}{\mathrm{NO}_y}-\frac{1}{2}R_{21}\frac{\mathrm{NMHC}^i}{\mathrm{NMHC}}-\frac{1}{2}R_{24}\frac{\mathrm{NMHC}^i}{\mathrm{NMHC}} \quad (21)\end{aligned}$$

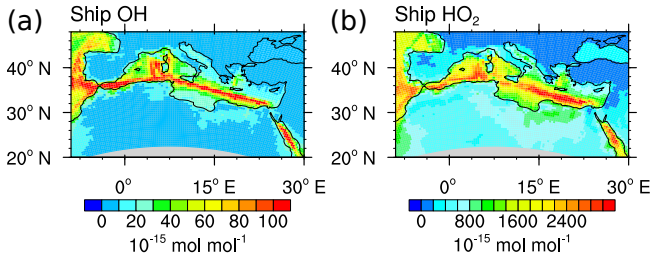

Figure 4. Contribution of shipping emissions to OH and HO_2 in 10^{-15} mol mol^{-1}. Monthly means of ground-level values in August 2007 are shown. Simulation is performed with MECO(n).

$$
\begin{aligned}
B^i = {} & \frac{1}{2} R_6 \frac{{O_3}^i}{O_3} + \frac{1}{2} R_7 \frac{{O_3}^i}{O_3} + \frac{1}{2} R_{11} \frac{CO^i}{CO} + R_{18} \frac{NO_y^i}{NO_y} \\
& + \frac{1}{2} R_{23} \left(\frac{NMHC^i}{NMHC} + \frac{NO_y^i}{NO_y} \right) + \frac{1}{2} R_{24} \frac{NMHC^i}{NMHC} \\
& + R_{25} \frac{NMHC^i}{NMHC} + R_{28} \frac{NMHC^i}{NMHC} - \frac{1}{2} R_4 \frac{{O_3}^i}{O_3} - \frac{1}{2} R_5 \frac{{O_3}^i}{O_3} \\
& - \frac{1}{2} R_{14} \frac{NO_y^i}{NO_y} - \frac{1}{2} R_{15} \frac{NO_y^i}{NO_y} - \frac{1}{2} R_{22} \frac{NMHC^i}{NMHC}
\end{aligned}
\tag{22}
$$

By solving Eqs. (15) and (16), we finally obtain the contributions of a source category i to the OH and HO_2 concentration (same equations as Eqs. 29 and 30 in Grewe et al., 2017, but with differently defined coefficients).

$$
\frac{OH^i}{OH} = \frac{A^i L^{HO_2} + B^i P^{OH}}{L^{OH} L^{HO_2} - P^{OH} P^{HO_2}} \tag{23}
$$

$$
\frac{{HO_2}^i}{HO_2} = \frac{A^i P^{HO_2} + B^i L^{OH}}{L^{OH} L^{HO_2} - P^{OH} P^{HO_2}} \tag{24}
$$

These equations are implemented in the TAGGING submodel, and EMAC and MECO(n) simulations according to Sect. 2 are performed. The results for the OH and HO_2 contributions are analysed and compared with V1.0 in the following section.

4 Results of model simulations

4.1 Contribution of short-lived species (HO_x)

Figures 2 and 3 show the zonal mean of OH and HO_2 contributions up to 200 hPa for the 10 source categories derived by V1.1 (first and third columns) and V1.0 (second and forth columns). The zonal mean of OH and HO_2 contributions from 1 to 200 hPa are shown in Appendix B (Figs. B1, B2). First, the OH and HO_2 contributions of V1.1 are described in the following. For the categories which are determined by anthropogenic emissions, such as shipping, road traffic and anthropogenic non-traffic, the maximum values of OH and HO_2 contributions occur in the lower troposphere in the Northern Hemisphere. This clearly shows that for anthropogenic-dominated categories the OH and HO_2 contributions are caused by anthropogenic emissions. The contributions vary among these categories of surface emissions as not only the amount but also the composition of the emissions differs. For the category aviation, maximum OH contributions are found in the Northern Hemisphere between 200 and 250 hPa. However, the HO_2 contribution has a minimum in this region and a maximum in the lower troposphere. The OH values for the categories CH_4 decomposition, N_2O decomposition, lightning and biogenic emissions are largest in the upper troposphere. Most OH contributions of biomass burning are found in the lower tropical troposphere. In contrast, negative values occur in the upper tropical troposphere. Concerning the HO_2 contribution, the residual categories show a maximum in the tropical lower troposphere. In addition, the category lightning shows a strong HO_2 loss in the upper tropical troposphere, which is caused by Reaction (14).

The results obtained by V1.1 are compared to the OH and HO_2 zonal profiles of V1.0 only in the troposphere (Figs. 2 and 3). The HO_x tagging method V1.0 was only developed for the troposphere. Hence, a comparison in the stratosphere is not reasonable. In general, contributions to OH and HO_2 concentrations of V1.1 are larger in the troposphere compared to V1.0. This overall shift towards larger values is explained by the re-establishment of the steady state and thus the closure of the budget in V1.1. In V1.0 the budget was not closed and thus the contributions were underestimated.

For OH, the categories lightning and aviation show no large changes in the general pattern of the zonal means between V1.0 and V1.1. Considering the HO_2 contributions, no large changes are found for the categories biomass burning, anthropogenic non-traffic, road traffic and shipping.

The contribution of the category aviation to HO_2 in V1.1 shows roughly the same pattern compared to V1.0. However, the HO_2 destruction along the flight path is no longer as pronounced, which is caused by the inclusion of Reactions (15) and (18) in V1.1. Reaction (15) adds the term $\frac{1}{2} R_{15} \frac{NO_y^i}{NO_y}$ to the HO_2 loss (Eq. 12) and Reaction (18) adds the term $R_{18} \frac{NO_y^i}{NO_y}$ to the HO_2 production (Eq. 11). As the reaction rate R_{15} equals the rate R_{18}, this leads to a larger HO_2 production than HO_2 loss $\left(R_{18} \frac{NO_y^i}{NO_y} > \frac{1}{2} R_{15} \frac{NO_y^i}{NO_y} \right)$. Consequently, the addition of Reactions (15) and (18) to the reduced HO_x reaction system V1.1 constitutes an extra HO_2 source.

Larger values of the categories N_2O decomposition and lightning to HO_2 in the upper troposphere are explained by a larger HO_2 production in V1.1 compared to V1.0. The H tagging in V1.1 considers all relevant HO_2 sources (Reac-

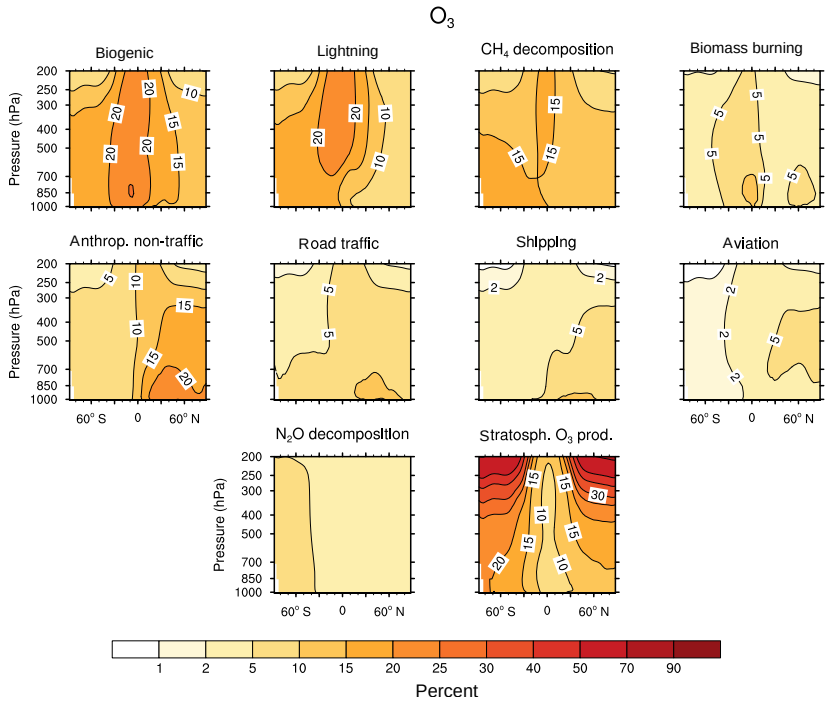

Figure 5. Annual mean contributions of 10 source categories to O_3 concentration in percent.

tions 7, 10, 11 and 28) leading to a larger HO_2 production. Also the addition of Reactions (15) and (18) (for an explanation see above) as well as the addition of Reaction (23), which considers more reactions than in V1.0, increases the HO_2 contribution of the categories N_2O decomposition and lightning.

Large changes in pattern are observed for the contributions of biogenic emissions and CH_4 decomposition to OH and HO_2 as well as for the contributions of biomass burning and anthropogenic non-traffic to OH. In V1.1, these categories mainly constitute a source of OH and HO_2 in the troposphere. The addition of Reactions (24) and (25) to the reduced HO_x reaction system V1.1 presents an HO_2 source increasing OH and HO_2 contributions. Furthermore, reactions of NMHC with OH, HO_2 and NO_y (Reactions 21, 22 and 23) are important throughout the whole troposphere. In contrast to V1.0, V1.1 considers all reactions of NMHC with OH, HO_2 and NO_y (see Sect. 3.2), significantly changing the pattern of biogenic emissions, CH_4 decomposition, biomass burning and anthropogenic non-traffic.

To demonstrate the impact of the advanced HO_x tagging method on a regional scale, Fig. 4 shows the contributions of ship emissions to OH and HO_2 in the boundary layer simulated with the high-resolution model MECO(n) (see Sect. 2). The ship paths in the Atlantic, Mediterranean and Red Sea are clearly visible and lead to OH and HO_2 production along these paths. In the polluted area at the coast of Marseille the OH and HO_2 contributions are reduced. In this region NO_y from shipping emissions is larger than in the Mediterranean Sea, causing a reduction of OH and HO_2 by Reactions (14) to (17).

The tagging method V1.0 (Grewe et al., 2017, their Fig. 6) showed negative HO_2 shipping contributions along the ship paths. This was explained by Reaction (14): NO destroys HO_2 and leads to negative contributions. However, in V1.1 HO_2 shipping contributions are positive. The change in sign is caused by the addition of Reactions (15) and (18) to the reduced HO_x reaction system V1.1, which constitutes a net HO_2 production, leading to positive HO_2 contributions (for an explanation see above). The comparison shows that HO_2 contributions in V1.0 were systematically and erroneously underestimated.

To summarize, the contributions to OH and HO_2 concentrations show larger values in V1.1 compared to V1.0. This is explained by the re-establishment of the steady state. For OH, no large changes are found in the categories lightning and aviation. However, large changes are found for biomass burning, CH_4 decomposition and biogenic emissions. For HO_2, no large differences occur in the categories biomass burning, anthropogenic non-traffic, road traffic and shipping. In comparison, the categories biogenic emissions and CH_4 decomposition differ strongly. The differences between the contributions of V1.1 and V1.0 are traced back to the addition of certain reactions to the reduced reaction system considered in the HO_x tagging method.

4.2 Effects on long-lived species

The tagging of short-lived and long-lived species closely intertwines (see Fig. 1). Changes in the contributions to OH and HO_2 influence the contributions to the long-lived tracers O_3, NO_y, CO, NMHC and PAN. For example, Fig. 5 shows the zonal mean of the contributions of the 10 source categories to O_3. Grewe et al. (2017) present the same figure for the HO_x tagging method V1.0 (their Fig. 4). For consistency, we compare our results with the results of Grewe et al. (2017) only for the year 2008.

In general, no large differences between V1.1 and V1.0 for long-lived species are found. The categories biogenic emissions and CH_4 decomposition show an O_3 increase in the tropical troposphere. Stratospheric O_3 production slightly increases in the Southern Hemisphere. Small O_3 changes are found for the categories lightning and N_2O decomposition. Regarding the remaining long-lived species (see Figs. S3–S6), the contribution of biomass burning to CO decreases, while the contributions of biogenic emissions to CO increase in the Southern Hemisphere. The remaining sectors stay rather unchanged. NO_y, NMHC and PAN show only minor changes. Even though major differences in OH and HO_2 occur between V1.0 and V1.1, these do not have a large effect on the long-lived species.

5 Discussion and conclusion

We present an extension of the HO_x tagging method described by Grewe et al. (2017). A total of 15 new reactions producing and destroying HO_x are added to the tagging mechanism. In Grewe et al. (2017), the HO_x tagging method V1.0 was restricted to the troposphere only. We further include the reactions which are essential for HO_x production and loss in the stratosphere. Moreover, we introduce an equivalent tagging method to obtain the contributions to the H radical. This step is mandatory to fully account for the main HO_2 source: the reaction of H with O_2.

In V1.0, the steady-state assumption was not completely fulfilled, resulting in an unclosed budget: the sum of the HO_x contributions and the total HO_x concentration deviated by about 70 %. To re-establish steady state, we add more reactions to the reduced HO_x reaction system and introduce rest terms to balance the deviation of HO_x production and loss. This leads to the closure of the budget. Thus, the tagging mechanism introduced by Grewe et al. (2010) operates not only for long-lived but also for short-lived species.

The advanced HO_x tagging method V1.1 was implemented in the global chemistry climate model EMAC and in the regional model MECO(n). A 1-year simulation was performed in both model systems and compared to V1.0. For most categories, the general zonal pattern of the contributions to OH and HO_2 show minor differences. In contrast, large changes are observed in the category biogenic emissions and CH_4 decomposition, which are traced back to the addition of certain reactions to V1.1. Although the contributions of long-lived and short-lived species influence each other, no large changes are found for long-lived species.

The mechanism presented in this study (and introduced by Tsati, 2014, and Grewe et al., 2017) is the first method for tagging short-lived species. Other studies quantify the source attributions of chemical species with a significantly longer lifetime. The idea of source attribution is applied to attribute CO to different emission types and regions (e.g. Granier et al., 1999; Pfister et al., 2004; Pfister et al., 2011), to attribute NO_x concentrations to emission sources (Horowitz and Jacob, 1999) or to trace stable isotopic compositions (Gromov et al., 2010). Also for the source attribution of tropospheric O_3, there are several tagging approaches attributing tropospheric O_3 only to NO_x sources (Lelieveld and Dentener, 2000; Grewe, 2004; Grewe et al., 2012; Emmons et al., 2012), only to NMHC sources (Butler et al., 2011; Coates and Butler, 2015) or to NO_y, CO and NMHC emissions simultaneously (Grewe et al., 2017).

A common technique to quantify the impact of emissions on OH is the so-called perturbation method, which compares two simulations: one simulation with all emissions and one simulation with reduced emissions (e.g. Niemeier et al., 2006; Hoor et al., 2009). However, if the underlying chemical processes are non-linear (as is the case for OH), the perturbation method largely underestimates the contribution (Grewe et al., 2012; Emmons et al., 2012; Mertens et al., 2018). Consequently, the tagging approach presented in this study delivers the actual contribution of the emission source, while the perturbation method displays the impact of the emission reduction.

To conclude, the further developed HO_x tagging method can be used to identify the contribution of anthropogenic emissions to the atmospheric composition. In particular, the contribution of emission sectors to the concentrations of OH and HO_2 in the troposphere and stratosphere can be measured. This method will be applied for re-evaluating the impact of the traffic sector on climate.

Code availability. The Modular Earth Submodel System (MESSy) is continuously further developed and applied by a consortium of institutions. The usage of MESSy and access to the source code is licensed to all affiliates of institutions which are members of the MESSy Consortium. Institutions can become a member of the MESSy Consortium by signing the MESSy Memorandum of Understanding. More information can be found on the MESSy Consortium website (http://www.messy-interface.org, last access: 22 May 2018). The submodel TAGGING 1.1 will be included in MESSy version 2.54. The code being used to obtain the presented results is available upon personal request.

Appendix A: Exclusion of reactions from reduced HO_x reaction system V1.1

The annual mean reaction rates of the following three reactions are also greater than 10^{-15} mol mol^{-1}s^{-1} and thus would usually be regarded in the reduced HO_x reaction system V1.1.

$$H_2O_2 + h\nu \longrightarrow 2OH \quad \text{(A1)}$$

$$HOCl + h\nu \longrightarrow OH + Cl \quad \text{(A2)}$$

$$HOBr + h\nu \longrightarrow OH + Br \quad \text{(A3)}$$

However, the tagging method cannot be applied for these three reactions.

To include the OH production by the photolysis of H_2O_2 (Reaction A1), we would need to tag H_2O_2. Since the production and the loss of H_2O_2 are not balanced, we cannot assume a steady state. Thus, a similar tagging approach as for HO_x and H is not valid for H_2O_2. Consequently, we exclude the Reaction (A1) from the HO_x tagging method. This reaction contributes about 8 % to the total OH production in the troposphere.

Hypochlorous acid (HOCl) and hypobromous acid (HOBr) are photolysed in the stratosphere and produce OH (Reactions A2 and A3), but HOCl and HOBr are not tagged. Although the steady-state assumption is globally valid, locally the production and loss of HOCl and HOBr are not balanced everywhere. In the stratosphere, for about 65 % of the model grid boxes the production deviates by more than 10 % from the loss of HOCl and HOBr. In particular, in the transition area between day and night in the polar region, the production deviates strongly from the loss. Also at night when the reactions mostly occur, the steady state is not fulfilled everywhere. Moreover, since both species are not radicals, their lifetimes cannot be assumed to be short. Hence, we cannot apply the tagging method, so we have to omit the Reactions (A2) and (A3) from the reduced HOx reaction system V1.1.

Considering Reactions (A1), (A2) and (A3) in the reduced HO_x reaction system V1.1 would lead to a significantly larger OH production in the troposphere representing about 98 % of the total OH production rate derived by MECCA. In the stratosphere, 91 % of the total OH production would be regarded. Hence, excluding these reactions from the reduced HO_x reaction system V1.1 worsens the steady-state assumption between OH production and loss. The rest term resOH introduced in Sect. 3.4 compensates for this deviation from the production and loss rate.

Appendix B: HO_x contributions in the stratosphere

Figures B1 and B2 show the zonal mean of OH and HO_2 from 1 to 200 hPa. As OH concentration strongly rises with increasing height, so do the contributions to OH. The category biomass burning shows negative OH values in the tropopause region. In this region, large CO values from biomass burning also occur. CO effectively destroys OH by Reaction (11), which causes this OH loss. The large OH loss in the lower stratosphere of the category stratospheric O_3 production is mainly caused by the destruction of OH by O_3 (Reaction 6).

The contributions to HO_2 in the stratosphere increases with height as well. The categories biogenic emissions, lightning, biomass burning, anthropogenic non-traffic, road traffic, shipping and aviation show a local maximum at around 5 hPa, which is caused by omitting the photolysis of HOCl (see Appendix A).

For the category lightning, HO_2 is destroyed by Reaction (14) in the tropopause region. The category N_2O decomposition shows negative values in the lower stratosphere and a strong negative minimum at around 10 hPa, which is also caused by Reaction (14). The local maximum with positive HO_2 contributions indicates that in this region the HO_2 production via Reactions (1) and (6) dominates the HO_2 loss via Reaction (14).

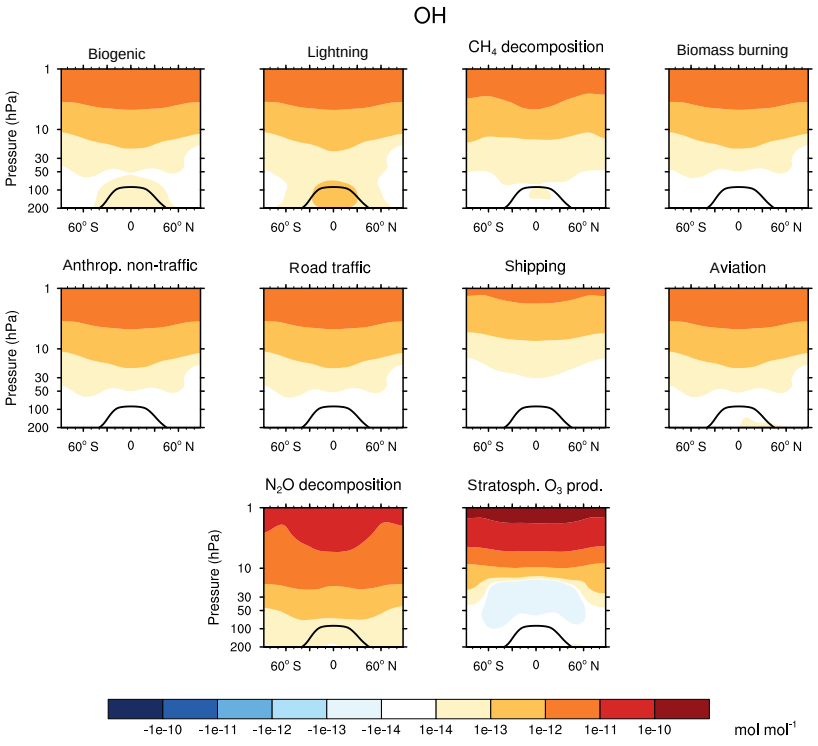

Figure B1. Contributions of 10 source categories to OH in the stratosphere. Zonal means of the year 2010 are shown. Black line indicates the tropopause. Simulation is performed with EMAC. Note the logarithmic scale of the contour levels.

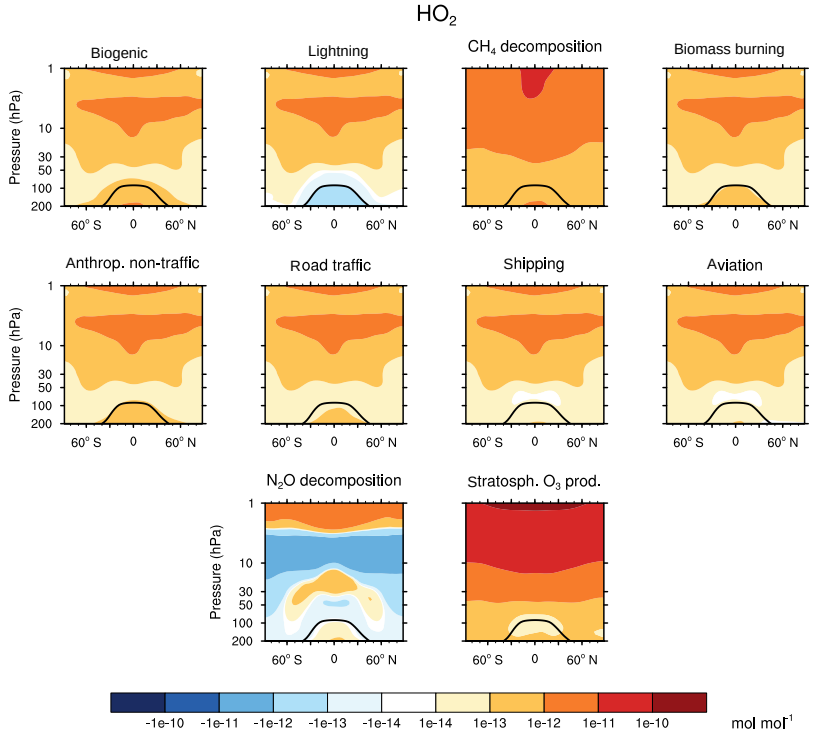

Figure B2. Contributions of 10 source categories to HO_2 in the stratosphere. Zonal means of the year 2010 are shown. Black line indicates the tropopause. Simulation is performed with EMAC. Note the logarithmic scale of the contour levels.

Supplement. The supplement related to this article is available online at: https://doi.org/10.5194/gmd-11-2049-2018-supplement.

Competing interests. There are no competing interests.

Acknowledgements. This study has been carried out in the framework of the project VEU2 funded by DLR. We used the NCAR Command Language (NCL) for data analysis and to create the figures of this study. NCL is developed by UCAR/NCAR/CISL/TDD and available online (DOI: 10.5065/D6WD3XH5). We gratefully acknowledge the computer systems provided by the Deutsches Klimarechenzentrum (DKRZ), which we used for our simulations. We thank Mattia Righi from DLR for helpful comments.

The article processing charges for this open-access publication were covered by a Research Centre of the Helmholtz Association.
Edited by: Olaf Morgenstern
Reviewed by: two anonymous referees

References

Butler, T., Lawrence, M., Taraborrelli, D., and Lelieveld, J.: Multi-day ozone production potential of volatile organic compounds calculated with a tagging approach, Atmos. Environ., 45, 4082–4090, https://doi.org/10.1016/j.atmosenv.2011.03.040, 2011.

Clappier, A., Belis, C. A., Pernigotti, D., and Thunis, P.: Source apportionment and sensitivity analysis: two methodologies with two different purposes, Geosci. Model Dev., 10, 4245–4256, https://doi.org/10.5194/gmd-10-4245-2017, 2017.

Coates, J. and Butler, T. M.: A comparison of chemical mechanisms using tagged ozone production potential (TOPP) analysis, Atmos. Chem. Phys., 15, 8795–8808, https://doi.org/10.5194/acp-15-8795-2015, 2015.

Crutzen, P. J. and Schmailzl, U.: Chemical budgets of the stratosphere, Planet. Space Sci., 31, 1009–1032, 1983.

Deckert, R., Jöckel, P., Grewe, V., Gottschaldt, K.-D., and Hoor, P.: A quasi chemistry-transport model mode for EMAC, Geosci. Model Dev., 4, 195–206, https://doi.org/10.5194/gmd-4-195-2011, 2011.

Emmons, L. K., Hess, P. G., Lamarque, J.-F., and Pfister, G. G.: Tagged ozone mechanism for MOZART-4, CAM-chem and other chemical transport models, Geosci. Model Dev., 5, 1531–1542, https://doi.org/10.5194/gmd-5-1531-2012, 2012.

Granier, C., Müller, J., Pétron, G., and Brasseur, G.: A three-dimensional study of the global CO budget, Chemosphere – Global Change Sci., 1, 255–261, https://doi.org/10.1016/S1465-9972(99)00007-0, 1999.

Granier, C., Bessagnet, B., Bond, T., D'Angiola, A., Denier van der Gon, H., Frost, G. J., Heil, A., Kaiser, J. W., Kinne, S., Klimont, Z., Kloster, S., Lamarque, J.-F., Liousse, C., Masui, T., Meleux, F., Mieville, A., Ohara, T., Raut, J.-C., Riahi, K., Schultz, M. G., Smith, S. J., Thompson, A., van Aardenne, J., van der Werf, G. R., and van Vuuren, D. P.: Evolution of anthropogenic and biomass burning emissions of air pollutants at global and regional scales during the 1980–2010 period, Clim. Change, 109, 163, https://doi.org/10.1007/s10584-011-0154-1, 2011.

Grewe, V.: Technical Note: A diagnostic for ozone contributions of various NO_x emissions in multi-decadal chemistry-climate model simulations, Atmos. Chem. Phys., 4, 729–736, https://doi.org/10.5194/acp-4-729-2004, 2004.

Grewe, V.: A generalized tagging method, Geosci. Model Dev., 6, 247–253, https://doi.org/10.5194/gmd-6-247-2013, 2013.

Grewe, V., Brunner, D., Dameris, M., Grenfell, J., Hein, R., Shindell, D., and Staehelin, J.: Origin and variability of upper tropospheric nitrogen oxides and ozone at northern mid-latitudes, Atmos. Environ., 35, 3421–3433, https://doi.org/10.1016/S1352-2310(01)00134-0, 2001.

Grewe, V., Tsati, E., and Hoor, P.: On the attribution of contributions of atmospheric trace gases to emissions in atmospheric model applications, Geosci. Model Dev., 3, 487–499, https://doi.org/10.5194/gmd-3-487-2010, 2010.

Grewe, V., Dahlmann, K., Matthes, S., and Steinbrecht, W.: Attributing ozone to NO_x emissions: Implications for climate mitigation measures, Atmos. Environ., 59, 102–107, https://doi.org/10.1016/j.atmosenv.2012.05.002, 2012.

Grewe, V., Tsati, E., Mertens, M., Frömming, C., and Jöckel, P.: Contribution of emissions to concentrations: the TAGGING 1.0 submodel based on the Modular Earth Submodel System (MESSy 2.52), Geosci. Model Dev., 10, 2615–2633, https://doi.org/10.5194/gmd-10-2615-2017, 2017.

Gromov, S., Jöckel, P., Sander, R., and Brenninkmeijer, C. A. M.: A kinetic chemistry tagging technique and its application to modelling the stable isotopic composition of atmospheric trace gases, Geosci. Model Dev., 3, 337–364, https://doi.org/10.5194/gmd-3-337-2010, 2010.

Guenther, A., Hewitt, C. N., Erickson, D., Fall, R., Geron, C., Graedel, T., Harley, P., Klinger, L., Lerdau, M., Mckay, W. A., Pierce, T., Scholes, B., Steinbrecher, R., Tallamraju, R., Taylor, J., and Zimmerman, P.: A global model of natural volatile organic compound emissions, J. Geophys. Res.-Atmos., 100, 8873–8892, https://doi.org/10.1029/94JD02950, 1995.

Heard, D. E. and Pilling, M. J.: Measurement of OH and HO_2 in the Troposphere, Chem. Rev., 103, 5163–5198, https://doi.org/10.1021/cr020522s, 2003.

Hoor, P., Borken-Kleefeld, J., Caro, D., Dessens, O., Endresen, O., Gauss, M., Grewe, V., Hauglustaine, D., Isaksen, I. S. A., Jöckel, P., Lelieveld, J., Myhre, G., Meijer, E., Olivie, D., Prather, M., Schnadt Poberaj, C., Shine, K. P., Staehelin, J., Tang, Q., van Aardenne, J., van Velthoven, P., and Sausen, R.: The impact of traffic emissions on atmospheric ozone and OH: results from QUANTIFY, Atmos. Chem. Phys., 9, 3113–3136, https://doi.org/10.5194/acp-9-3113-2009, 2009.

Horowitz, L. W. and Jacob, D. J.: Global impact of fossil fuel combustion on atmospheric NO_x, J. Geophys. Res.-Atmos., 104, 23823–23840, https://doi.org/10.1029/1999JD900205, 1999.

Jöckel, P., Kerkweg, A., Pozzer, A., Sander, R., Tost, H., Riede, H., Baumgaertner, A., Gromov, S., and Kern, B.: Development cycle 2 of the Modular Earth Submodel System (MESSy2), Geosci. Model Dev., 3, 717–752, https://doi.org/10.5194/gmd-3-717-2010, 2010.

Jöckel, P., Tost, H., Pozzer, A., Kunze, M., Kirner, O., Brenninkmeijer, C. A. M., Brinkop, S., Cai, D. S., Dyroff, C., Eckstein, J., Frank, F., Garny, H., Gottschaldt, K.-D., Graf, P., Grewe, V., Kerkweg, A., Kern, B., Matthes, S., Mertens, M., Meul, S., Neumaier, M., Nützel, M., Oberländer-Hayn, S., Ruhnke, R., Runde,

T., Sander, R., Scharffe, D., and Zahn, A.: Earth System Chemistry integrated Modelling (ESCiMo) with the Modular Earth Submodel System (MESSy) version 2.51, Geosci. Model Dev., 9, 1153–1200, https://doi.org/10.5194/gmd-9-1153-2016, 2016.

Kerkweg, A. and Jöckel, P.: The 1-way on-line coupled atmospheric chemistry model system MECO(n) – Part 1: Description of the limited-area atmospheric chemistry model COSMO/MESSy, Geosci. Model Dev., 5, 87–110, https://doi.org/10.5194/gmd-5-87-2012, 2012a.

Kerkweg, A. and Jöckel, P.: The 1-way on-line coupled atmospheric chemistry model system MECO(n) – Part 2: On-line coupling with the Multi-Model-Driver (MMD), Geosci. Model Dev., 5, 111–128, https://doi.org/10.5194/gmd-5-111-2012, 2012b.

Kerkweg, A., Sander, R., Tost, H., and Jöckel, P.: Technical note: Implementation of prescribed (OFFLEM), calculated (ONLEM), and pseudo-emissions (TNUDGE) of chemical species in the Modular Earth Submodel System (MESSy), Atmos. Chem. Phys., 6, 3603–3609, https://doi.org/10.5194/acp-6-3603-2006, 2006.

Lawrence, M. G., Jöckel, P., and von Kuhlmann, R.: What does the global mean OH concentration tell us?, Atmos. Chem. Phys., 1, 37–49, https://doi.org/10.5194/acp-1-37-2001, 2001.

Lelieveld, J. and Dentener, F. J.: What controls tropospheric ozone?, J. Geophys. Res.-Atmos., 105, 3531–3551, https://doi.org/10.1029/1999JD901011, 2000.

Liang, Q., Chipperfield, M. P., Fleming, E. L., Abraham, N. L., Braesicke, P., Burkholder, J. B., Daniel, J. S., Dhomse, S., Fraser, P. J., Hardiman, S. C., Jackman, C. H., Kinnison, D. E., Krummel, P. B., Montzka, S. A., Morgenstern, O., McCulloch, A., Mühle, J., Newman, P. A., Orkin, V. L., Pitari, G., Prinn, R. G., Rigby, M., Rozanov, E., Stenke, A., Tummon, F., Velders, G. J. M., Visioni, D., and Weiss, R. F.: Deriving Global OH Abundance and Atmospheric Lifetimes for Long-Lived Gases: A Search for CH_3CCl_3 Alternatives, J. Geophys. Res.-Atmos., 122, 11,914–11,933, https://doi.org/10.1002/2017JD026926, 2017.

Mertens, M., Kerkweg, A., Jöckel, P., Tost, H., and Hofmann, C.: The 1-way on-line coupled model system MECO(n) – Part 4: Chemical evaluation (based on MESSy v2.52), Geosci. Model Dev., 9, 3545–3567, https://doi.org/10.5194/gmd-9-3545-2016, 2016.

Mertens, M., Grewe, V., Rieger, V. S., and Jöckel, P.: Revisiting the contribution of land transport and shipping emissions to tropospheric ozone, Atmos. Chem. Phys., 18, 5567–5588, https://doi.org/10.5194/acp-18-5567-2018, 2018.

Montzka, S. A., Krol, M., Dlugokencky, E., Hall, B., Jöckel, P., and Lelieveld, J.: Small Interannual Variability of Global Atmospheric Hydroxyl, Science, 331, 67–69, https://doi.org/10.1126/science.1197640, 2011.

Naik, V., Voulgarakis, A., Fiore, A. M., Horowitz, L. W., Lamarque, J.-F., Lin, M., Prather, M. J., Young, P. J., Bergmann, D., Cameron-Smith, P. J., Cionni, I., Collins, W. J., Dalsøren, S. B., Doherty, R., Eyring, V., Faluvegi, G., Folberth, G. A., Josse, B., Lee, Y. H., MacKenzie, I. A., Nagashima, T., van Noije, T. P. C., Plummer, D. A., Righi, M., Rumbold, S. T., Skeie, R., Shindell, D. T., Stevenson, D. S., Strode, S., Sudo, K., Szopa, S., and Zeng, G.: Preindustrial to present-day changes in tropospheric hydroxyl radical and methane lifetime from the Atmospheric Chemistry and Climate Model Intercomparison Project (ACCMIP), Atmos. Chem. Phys., 13, 5277–5298, https://doi.org/10.5194/acp-13-5277-2013, 2013.

Niemeier, U., Granier, C., Kornblueh, L., Walters, S., and Brasseur, G. P.: Global impact of road traffic on atmospheric chemical composition and on ozone climate forcing, J. Geophys. Res.-Atmos., 111, d09301, https://doi.org/10.1029/2005JD006407, 2006.

Olson, J. R., Crawford, J. H., Chen, G., Brune, W. H., Faloona, I. C., Tan, D., Harder, H., and Martinez, M.: A reevaluation of airborne HOx observations from NASA field campaigns, J. Geophys. Res.-Atmos., 111, d10301, https://doi.org/10.1029/2005JD006617, 2006.

Pfister, G., Pétron, G., Emmons, L. K., Gille, J. C., Edwards, D. P., Lamarque, J.-F., Attie, J.-L., Granier, C., and Novelli, P. C.: Evaluation of CO simulations and the analysis of the CO budget for Europe, J. Geophys. Res.-Atmos., 109, d19304, https://doi.org/10.1029/2004JD004691, 2004.

Pfister, G. G., Avise, J., Wiedinmyer, C., Edwards, D. P., Emmons, L. K., Diskin, G. D., Podolske, J., and Wisthaler, A.: CO source contribution analysis for California during ARCTAS-CARB, Atmos. Chem. Phys., 11, 7515–7532, https://doi.org/10.5194/acp-11-7515-2011, 2011.

Prinn, R. G., Huang, J., Weiss, R. F., Cunnold, D. M., Fraser, P. J., Simmonds, P. G., McCulloch, A., Harth, C., Reimann, S., Salameh, P., O'Doherty, S., Wang, R. H. J., Porter, L. W., Miller, B. R., and Krummel, P. B.: Evidence for variability of atmospheric hydroxyl radicals over the past quarter century, Geophysical Research Letters, 32, l07809, https://doi.org/10.1029/2004GL022228, 2005.

Ren, X., Harder, H., Martinez, M., Lesher, R. L., Oliger, A., Simpas, J. B., Brune, W. H., Schwab, J. J., Demerjian, K. L., He, Y., Zhou, X., and Gao, H.: OH and HO_2 Chemistry in the urban atmosphere of New York City, Atmos. Environ., 37, 3639–3651, https://doi.org/10.1016/S1352-2310(03)00459-X, 2003.

Righi, M., Eyring, V., Gottschaldt, K.-D., Klinger, C., Frank, F., Jöckel, P., and Cionni, I.: Quantitative evaluation of ozone and selected climate parameters in a set of EMAC simulations, Geosci. Model Dev., 8, 733–768, https://doi.org/10.5194/gmd-8-733-2015, 2015.

Roeckner, E., Brokopf, R., Esch, M., Giorgetta, M., Hagemann, S., Kornblueh, L., Manzini, E., Schlese, U., and Schulzweida, U.: Sensitivity of Simulated Climate to Horizontal and Vertical Resolution in the ECHAM5 Atmosphere Model, J. Climate, 19, 3771–3791, https://doi.org/10.1175/JCLI3824.1, 2006.

Sander, R., Baumgaertner, A., Gromov, S., Harder, H., Jöckel, P., Kerkweg, A., Kubistin, D., Regelin, E., Riede, H., Sandu, A., Taraborrelli, D., Tost, H., and Xie, Z.-Q.: The atmospheric chemistry box model CAABA/MECCA-3.0, Geosci. Model Dev., 4, 373–380, https://doi.org/10.5194/gmd-4-373-2011, 2011.

Stevenson, D. S., Dentener, F. J., Schultz, M. G., Ellingsen, K., van Noije, T. P. C., Wild, O., Zeng, G., Amann, M., Atherton, C. S., Bell, N., Bergmann, D. J., Bey, I., Butler, T., Cofala, J., Collins, W. J., Derwent, R. G., Doherty, R. M., Drevet, J., Eskes, H. J., Fiore, A. M., Gauss, M., Hauglustaine, D. A., Horowitz, L. W., Isaksen, I. S. A., Krol, M. C., Lamarque, J.-F., Lawrence, M. G., Montanaro, V., Müller, J.-F., Pitari, G., Prather, M. J., Pyle, J. A., Rast, S., Rodriguez, J. M., Sanderson, M. G., Savage, N. H., Shindell, D. T., Strahan, S. E., Sudo, K., and Szopa, S.: Multimodel ensemble simulations of present-day and

near-future tropospheric ozone, J. Geophys. Res.-Atmos., 111, d08301, https://doi.org/10.1029/2005JD006338, 2006.

Stone, D., Whalley, L. K., and Heard, D. E.: Tropospheric OH and HO_2 radicals: field measurements and model comparisons, Chem. Soc. Rev., 41, 6348–6404, https://doi.org/10.1039/C2CS35140D, 2012.

Tsati, E. E.: Investigation of the impacts of emissions on the trace gas budgets in the troposphere by using global climate chemistry model simulations, Ph.D. thesis, Ludwig-Maximilians-Universität München, available at: https://edoc.ub.uni-muenchen.de/17524/ (last access: 27 October 2014), 2014.

Voulgarakis, A., Naik, V., Lamarque, J.-F., Shindell, D. T., Young, P. J., Prather, M. J., Wild, O., Field, R. D., Bergmann, D., Cameron-Smith, P., Cionni, I., Collins, W. J., Dalsøren, S. B., Doherty, R. M., Eyring, V., Faluvegi, G., Folberth, G. A., Horowitz, L. W., Josse, B., MacKenzie, I. A., Nagashima, T., Plummer, D. A., Righi, M., Rumbold, S. T., Stevenson, D. S., Strode, S. A., Sudo, K., Szopa, S., and Zeng, G.: Analysis of present day and future OH and methane lifetime in the ACCMIP simulations, Atmos. Chem. Phys., 13, 2563–2587, https://doi.org/10.5194/acp-13-2563-2013, 2013.

Yienger, J. J. and Levy, H.: Empirical model of global soil-biogenic NO_x emissions, J. Geophys. Res.-Atmos., 100, 11447–11464, https://doi.org/10.1029/95JD00370, 1995.